

Numerical Simulation of ZnO-Based Terahertz Quantum Cascade Lasers

ENRICO BELLOTTI^{1,2} and ROBERTO PAIELLA¹

1.—Department of Electrical and Computer Engineering and Photonics Center, Boston University, 8 Saint Mary's Street, Boston, MA 02215, USA. 2.—e-mail: bellotti@bu.edu

In this work, a particle-based Monte Carlo model is used to quantify the potential of terahertz sources based on the ZnO-based material system relative to existing devices based on GaAs/AlGaAs quantum wells. Specifically, two otherwise identical quantum cascade structures based on ZnO/MgZnO and GaAs/AlGaAs quantum wells are designed, and their non-equilibrium carrier distributions are then computed as a function of temperature. The simulation results show that, because of their larger optical phonon energy, ZnO/MgZnO quantum cascade laser structures exhibit weaker temperature dependence of the population inversion than in the case of similar structures made of GaAs/AlGaAs. In particular, as the temperature is increased from 10 K to 300 K, population inversion is found to decrease by a factor of 4.48 and 1.50 for the AlGaAs and MgZnO structure, respectively. Based on these results, the MgZnO devices are then predicted to be, in principle, capable of laser action without cryogenic cooling.

Key words: Terahertz, quantum cascade laser, Monte Carlo, zinc oxide

INTRODUCTION

The terahertz (THz) spectral region, defined as the frequency range between 300 GHz and 10 THz, corresponding to wavelengths between 1 mm and 30 μm , has so far remained largely unutilized due to the lack of practical sources and detectors.¹ THz technologies could find use in many sensing, spectroscopy, and imaging applications, because of the ability of THz light to penetrate through many packaging materials with little attenuation, and due to the presence of distinctive rotational/vibrational resonances at THz frequencies in many complex molecules of interest. To achieve widespread application of these THz-based technologies, practical semiconductor devices for generation, processing, and detection of THz light have to be developed.

The first THz semiconductor laser based on the quantum cascade (QC) scheme was reported in 2002.² In this kind of device, light emission involves

intersubband (ISB) transitions in quantum wells (QWs).³ This approach makes it possible to tune the emission wavelength over a broad spectral range through the design of the QW active material. Since 2002, THz QC lasers based on GaAs/AlGaAs QWs have made remarkable progress^{4–8} and can now cover the frequency range between 1.2 THz and 5 THz, often with output powers of several milliwatts. The operation of these GaAs/AlGaAs devices fundamentally requires cryogenic cooling, with maximum temperatures reported so far near 186 K and 120 K for pulsed and continuous-wave emission, respectively.⁹ Furthermore, their present wavelength coverage cannot be extended much further into the high-frequency side of the THz region. Both of these limitations are intrinsic, as they are related to the presence in (Al)GaAs of optical phonon modes with THz frequencies (e.g., $\nu_{\text{LO}} \approx 8.2$ THz in GaAs). This results in a large absorption mechanism for light at the same frequencies (*reststrahlen* absorption) and an ultrafast nonradiative decay mechanism between laser subbands separated by THz-range energies. These phenomena prevent operation of GaAs-based THz

(Received November 1, 2009; accepted March 16, 2010; published online May 11, 2010)

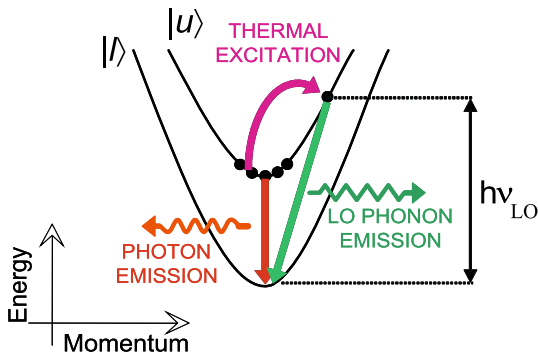


Fig. 1. Schematic illustration of the competition between photon emission and thermally activated LO-phonon emission by electrons in the upper laser subband of a THz QC structure.

QC lasers at frequencies within and immediately around the ~ 8 THz to 9 THz GaAs *reststrahlen* band. While GaAs/AlGaAs QC lasers emitting at lower frequencies can be realized, they are limited to operation at cryogenic temperatures, due to the process of thermally activated LO-phonon emission.

This nonradiative decay mechanism is illustrated schematically in Fig. 1, which shows the dispersion curves of the upper and lower laser subbands (labeled $|u\rangle$ and $|l\rangle$, respectively) of a generic THz QC structure. Laser action in this active material involves selective injection of electrons into the upper subband $|u\rangle$. At cryogenic temperatures the majority of these electrons occupy states near the bottom of the subband, from which they cannot decay nonradiatively into $|l\rangle$ via LO-phonon emission if $\nu < \nu_{\text{LO}}$, because of the requirement of energy conservation; as a result, a large population inversion can be established. As the temperature is increased, however, more and more of the electrons in $|u\rangle$ gain enough thermal energy that scattering into $|l\rangle$ via LO-phonon emission becomes allowed. Since these scattering processes are ultrafast, the end result is a dramatic reduction in device population inversion and optical gain.

It follows from this argument that, the closer the laser emission frequency ν to the LO-phonon frequency ν_{LO} of the QW materials, the more effectively population inversion is degraded with increasing temperature. In particular, THz QC laser action at room temperature, T_{rt} , will likely require that the energy difference $h\nu_{\text{LO}} - h\nu$ be significantly larger than the thermal energy $k_{\text{B}}T_{\text{rt}} \approx 26$ meV, so that LO-phonon-assisted nonradiative decay from $|u\rangle$ to $|l\rangle$ is disallowed even to (most) thermally excited electrons in $|u\rangle$. In GaAs wells, where $h\nu_{\text{LO}} \approx 36$ meV, the above condition is not fully satisfied at any THz emission frequency. Therefore it is likely that further progress in the high-temperature performance of THz injection lasers will require novel heterostructures featuring larger LO-phonon frequencies. Suitable materials may be found among wide-bandgap semiconductors, in which the strongly ionic chemical bonds lead to

phonon optical modes with high oscillation frequencies. A promising materials system in this respect is that of ZnO/MgZnO QWs, where the LO-phonon energy is about 72 meV. These heterostructures are currently the subject of extensive research, primarily aimed at the development of ultraviolet light-emitting diodes and lasers based on excitonic interband transitions. Although their material and device technology is at an earlier stage compared with other wide-bandgap material systems (for example, GaN/AlGaAs QWs), they could have some potential advantages, including generally smaller lattice mismatch and weaker polarization fields. ISB transitions in ZnO/MgZnO QWs have only been measured in one recent report,¹⁰ where photocurrent spectroscopy was used to identify ISB absorption peaks at mid-infrared wavelengths.

This article is organized as follows. In the second section, we briefly describe the ZnO material system. Subsequently in the third section, we present the gain medium design of two nominally “identical” THz QC structures based on GaAs/AlGaAs and ZnO/MgZnO QWs and describe the Monte Carlo approach used to study carrier dynamics in these structures. In the fourth section, this Monte Carlo model is used to compute the steady-state carrier distributions of the two QC structures under study as functions of temperature. The article then concludes with a brief discussion of the technological challenges involved in the experimental demonstration of these new devices.

THE ZnO MATERIAL SYSTEM

ZnO is used in a variety of technological applications, for example, piezoelectric transducers,¹¹ and has received a lot of attention, because of its excitonic properties and its potential for use as a transparent conductor in solar cell systems for photovoltaic power generation. Various studies have been carried out to determine its crystal properties and electronic structure,^{12–14} including the valence band ordering.¹⁴ Since it grows predominantly in the wurtzite form, the crystal polarity^{15–17} and the associated surface properties¹⁸ as well as the lattice dynamics^{19,20} have also been investigated. Since polytypes other than wurtzite can be present, depending on the growth conditions, the issue of phase transformation has also received attention.²¹ Extensive studies have been performed on the optical properties of ZnO,^{22,23} particularly the excitonic transition, and their potential applications.²⁴ In spite of continuous improvements in the techniques used,^{25–31} *p*-type doping remains one of the most important issues to be resolved for fabrication of reliable ZnO electronic and optoelectronic devices.

In spite of their importance for device design, the transport properties of ZnO have received little attention,^{25,32–35} and only recently has the first

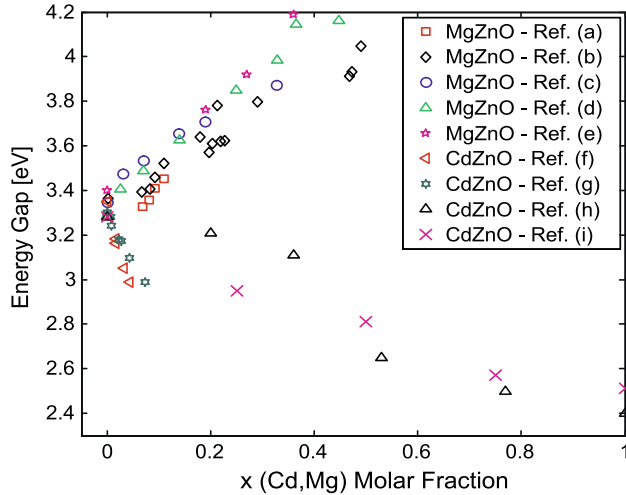


Fig. 2. Experimental measurements of the energy gap in $\text{Mg}_x\text{Zn}_{1-x}\text{O}$ films: Refs. 46 (a), 46 (b), 45 (c), 45 (d), 47 and 48 (e), and $\text{Cd}_x\text{Zn}_{1-x}\text{O}$ films: Refs. 51 (f), 52 (g), 37 (h), and 53 (i).

comprehensive investigation of ZnO transport coefficients been performed.^{35,36}

Much less work has been done on ZnO ternary compound semiconductors. The substitution of Zn with magnesium (Mg) or beryllium (Be) to form $\text{Mg}_x\text{Zn}_{1-x}\text{O}$ and $\text{Be}_x\text{Zn}_{1-x}\text{O}$ has produced ternary alloys with larger bandgaps than ZnO,^{37,38} while substituting Zn with Cd results in $\text{Cd}_x\text{Zn}_{1-x}\text{O}$, which has a smaller bandgap. Anion isovalent substitution in ZnO, i.e., replacing oxygen (O) with sulfur (S), has been reported recently.^{39–44}

The $\text{Mg}_x\text{Zn}_{1-x}\text{O}$ alloy has been considered as a suitable material for the barrier layers in ZnO/MgZnO heterostructures, because alloying ZnO with MgO enables widening of the bandgap of ZnO. Since ZnO has a wurtzite structure while MgO has a cubic structure, the ternary alloy is likely to undergo phase segregation. Several research groups^{45–50} have reported $\text{Mg}_x\text{Zn}_{1-x}\text{O}$ films fabricated using a variety of techniques. Figure 2 presents currently available experimental measurements of the energy gap as a function of the Mg molar fraction in $\text{Mg}_x\text{Zn}_{1-x}\text{O}$. In all of these cases, the crystals were reported to have wurtzite structure. The bandgap energy tends to increase linearly (i.e., with bowing parameter $b = 0$) with x up to 4.15 eV for $x = 0.36$ and saturates at higher Mg concentrations due to MgO segregation. This indicates that $\text{Mg}_x\text{Zn}_{1-x}\text{O}$ is a suitable material for barrier layers in ZnO/(Mg,ZnO) heterostructures with a bandgap offset of up to 0.85 eV.

It has only recently become possible to synthesize $\text{Be}_x\text{Zn}_{1-x}\text{O}$.^{38,54} The advantage of using BeO to obtain a ternary alloy stems from its wurtzite structure. This makes it possible to obtain a compound with a bandgap that can be continuously varied between ZnO and BeO (10.6 eV) without phase segregation. Figure 3 presents the measured $\text{Be}_x\text{Zn}_{1-x}\text{O}$ energy gap as a function of composition.

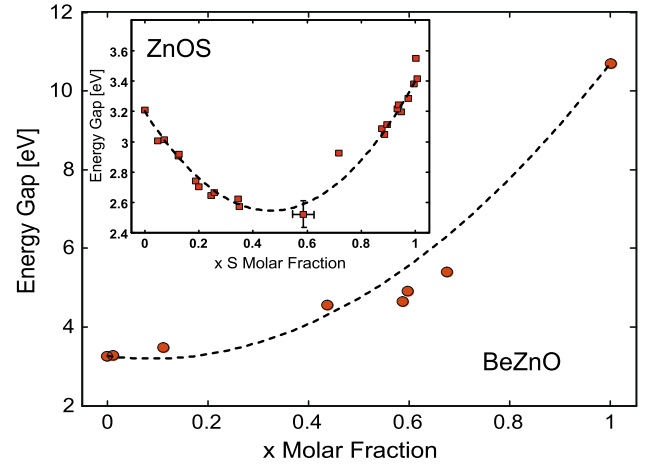


Fig. 3. Experimental measurements of the energy gap in $\text{Be}_x\text{Zn}_{1-x}\text{O}$ films as a function of composition.³⁸ Inset: measured fundamental energy gap of $\text{ZnO}_{1-x}\text{S}_x$ as a function of composition.⁴²

Narrowing of the bandgap is desirable to allow tuning of the emission wavelength of future ZnO-based optoelectronic devices into the visible spectral range. The ternary alloy $\text{Cd}_x\text{Zn}_{1-x}\text{O}$ is a potential candidate material, because of the smaller direct bandgap of CdO of 2.3 eV.^{55,56} Figure 2 summarizes the experimental energy bandgap data currently available for $\text{Cd}_x\text{Zn}_{1-x}\text{O}$.

In this work we use ZnO/MgZnO-based QWs because, among all the ternary alloys of this materials system, MgZnO is the most technologically developed. Furthermore, the conduction band discontinuity offered by MgZnO barrier layers provides carrier confinement suitable for the design of the QC structure studied in this work.

DEVICE DESIGN AND SIMULATION

The QC gain media studied in this work were designed using a Schrödinger equation solver based on the effective-mass approximation.⁵⁷ Their conduction-band profiles under optimal bias conditions are plotted in Fig. 4a and b, together with the squared envelope functions of the relevant bound states (referenced to their respective energy levels). The conduction-band diagrams of Fig. 4 were computed by solving the following Schrödinger equations (Eq. 1 and Eq. 2) in the well and barrier layers, respectively, together with standard boundary conditions of quantum mechanics:

$$\left[-\frac{\hbar^2}{2m_c^w} \frac{d^2}{dz^2} + e(F_{\text{ext}} + F_{\text{int}}^w)z \right] \phi(z) = E\phi(z), \quad (1)$$

$$\left[-\frac{\hbar^2}{2m_c^b} \frac{d^2}{dz^2} + \Delta E_c + e(F_{\text{ext}} + F_{\text{int}}^b)z \right] \phi(z) = E\phi(z). \quad (2)$$

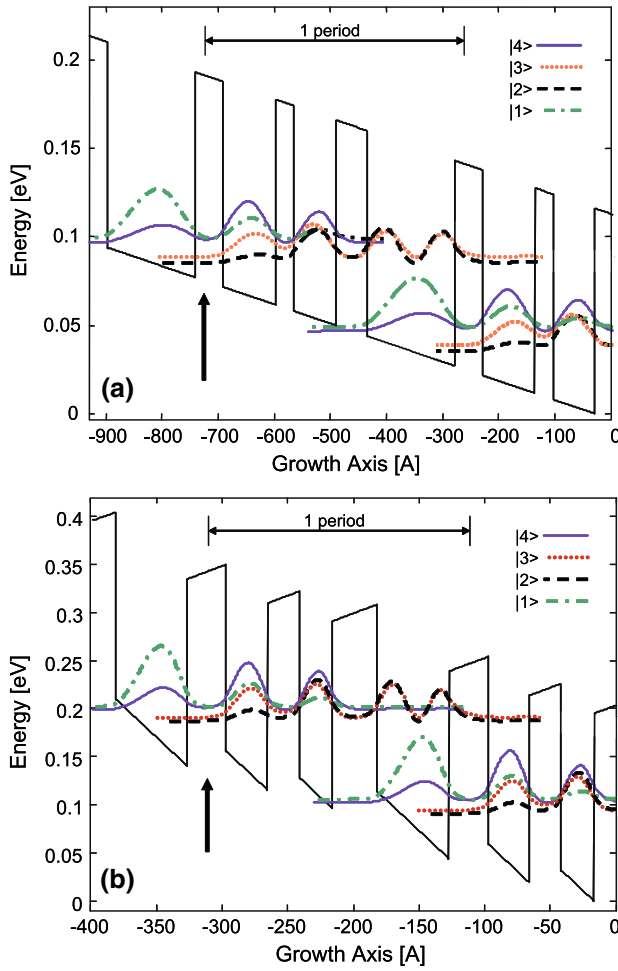


Fig. 4. Conduction-band profile and squared envelope functions of (a) the GaAs/Al_{0.15}Ga_{0.85}As and (b) the ZnO/Mg_{0.15}Zn_{0.85}O QC gain media considered in this study.

The numerical values used for the relevant material parameters of the QWs under study are listed in Table I. As can be seen in Fig. 4a and b, for the ZnO/Mg_{0.15}Zn_{0.85}O structure the presence of the spontaneous and piezoelectric polarization causes the bands in the well to tilt in the opposite direction to the bands in the barrier. The two structures in Fig. 4a and b consist of GaAs/Al_{0.15}Ga_{0.85}As and ZnO/Mg_{0.15}Zn_{0.85}O well/barrier combinations, respectively. In the former case, the barrier composition was chosen in accordance with most experimental demonstrations of GaAs THz QC lasers reported so far.^{2,4-8} In the case of the ZnO structure, it was selected to produce a similar degree of quantum confinement of the subbands involved in the laser action. In particular, the energy separation between the manifold of excited states |2>–|4> in each repeat unit and the *average* conduction-band edge of the injection barrier downstream is approximately the same in both structures, around 50 meV. By coincidence, this criterion is consistent with the same concentration (15%) of the additional element in the barrier alloy.

Table I. Summary of the material parameters used in the simulations presented in this work

	GaAs/Al _{0.15} Ga _{0.85} As	ZnO/Mg _{0.15} Zn _{0.85} O
m_c^w	0.067	0.24
m_c^b	0.079	–
ε_s^w	13.18	8.1
ε_s^b	12.71	–
ε_∞^w	10.89	4.11
ΔE_c (meV)	116	208
ΔP (C m ⁻²)	0	0.0014
$\hbar\omega_{LO}^w$ (meV)	36.25	72.0

The superscripts “w” and “b” denote the well and barrier material, respectively.

The layer thicknesses of a single repeat unit, starting from the injection barrier (indicated by the arrow) and moving downstream, are **49 Å/94 Å/33 Å/74 Å/56 Å/156 Å** for the GaAs structure and **30 Å/31 Å/25 Å/24 Å/34 Å/55 Å** for the ZnO structure, where the bold numbers refer to the barrier layers. The externally applied electric field F_{ext} in each plot is selected to produce a situation of near anticrossing between the lowest subband |1> of each repeat unit and subband |4> of the unit downstream. The specific values are 11 kV/cm and 48 kV/cm for the GaAs and ZnO device, respectively.

In order to obtain the fairest possible comparison between the materials systems under consideration, these two gain media were designed based on the same scheme, i.e., a variation of the “resonant-phonon” THz QC design⁵ involving only three QWs per repeat unit.⁷ The optical transitions occur between the subbands labeled |4> and |3> in each repeat unit of the active materials. The lower laser states are rapidly depopulated through tunneling into state |2> downstream and scattering into state |1> via resonant LO-phonon emission. To maximize the speed of the latter process, the energy separation between subbands |2> and |1> is close to the LO-phonon energy of the well material. At the same time, the spatial overlap between states |4> and |1> in each repeat unit is kept as small as possible, to avoid fast depopulation of the latter (at least at low temperatures). This QC design scheme has been successfully demonstrated with a recent GaAs/AlGaAs device,⁷ and was chosen for this study because of its inherent simplicity. Also for the sake of a fair comparison, the two gain media of Fig. 4 feature the same target emission frequency of 2 THz (8.2 meV), chosen because it lies in a window of relatively high atmospheric transmission within the THz spectrum.

The carrier dynamics in the two gain media has been studied using a particle-based Monte Carlo approach⁵⁷ with the aim of determining the steady-state carrier distributions of the laser subbands as a function of temperature, starting from a constant

population initially assigned to each subband. This approach has already been applied to study the carrier dynamics and the population inversion characteristics in other QC structures.^{2,58–60} Typically several thousand particles per subband are simulated, and specifically the results presented in the fourth section have been obtained using an ensemble of 5000 electrons per subband. Initially the particles are assigned in equal number to each subband according to a thermal distribution. The ensemble is subsequently allowed to evolve, and the simulation is terminated when the population of each subband remains unchanged for a given number of iteration steps. Convergence is checked both with respect to each subband within a single repeat unit and between identical subbands in different repeat units. Each iteration step involves a number of subhistories in which the state of each particle evolves for a given time and the distribution-function-based statistics are updated.

The numerical model for the device structures studied in this work includes 4 subbands per period, and 3 adjacent periods are simulated for a total of 12 subbands. Periodic boundary conditions are applied such that, for each particle exiting the third repeat unit, a new one is injected in the first. Electron/electron and electron/LO-phonon scattering are both included in the simulations^{61–63} with the relevant scattering rates at a given temperature computed and stored for each subband pair for a discrete number of initial electron \mathbf{k} -vectors (energies). When convergence is reached, the populations of the relevant subbands are computed and used to determine the inversion.

SIMULATION RESULTS

Using the simulation model just described we have calculated the steady-state carrier distributions of the two QC structures under study as a function of operating temperature. From the calculated carrier density in each subband at each temperature it is possible to compute the population inversion.

Figure 5 presents the calculated fractional population inversion $\Delta n = (n_4 - n_3)/n_{\text{tot}}$ versus temperature for the two structures shown in Fig. 4a and b. Here, n_4 and n_3 are the sheet electron densities of the upper and lower laser subbands, as computed from their respective nonequilibrium distribution functions, and n_{tot} is the total electron density per period, which in this calculation has been taken to be $2 \times 10^{10} \text{ cm}^{-2}$. The results plotted in this figure fully support and quantify the claim that ZnO THz QC structures can provide better performance compared with GaAs gain media.

In particular, Δn in the ZnO structure is found to degrade much more slowly with increasing temperature compared with the GaAs device. For example, as the temperature is increased from 10 K to 300 K, Δn in the ZnO structure decreases only by

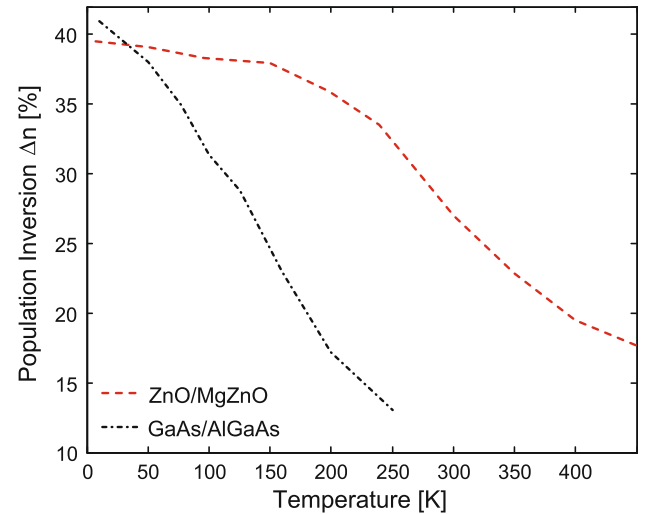


Fig. 5. Calculated fractional population inversion of the terahertz QC structures of Fig. 4a (dash-dotted line) and Fig. 4b (dashed line), as a function of temperature.

a factor of 1.50, versus 4.48 in the GaAs gain medium. The latter result is consistent with the severe performance degradation with increasing temperature that is observed experimentally in GaAs THz QC lasers, which is caused by thermally activated LO-phonon emission and (to a lesser extent⁶) by thermal backfilling of the lower laser states from the states downstream. Both of these limiting factors are much less effective in the presence of the large LO-phonon energies of ZnO/MgZnO QWs, as clearly indicated by our simulation results.

The maximum operating temperatures of the two gain media can be estimated from the plots of Fig. 5 as the temperatures beyond which Δn is smaller than the population inversion required to reach the lasing threshold. In QC lasers, the latter quantity can be written as follows⁶⁴:

$$\Delta n_{\text{th}} = \frac{1}{n_{\text{tot}}} \frac{\alpha \epsilon_0 \eta c \gamma L_p}{\Gamma N_p \hbar \omega (qz)^2}, \quad (3)$$

where η is the refractive index, γ is the full-width at half-maximum of the gain spectrum, L_p is the length of one period of the active material, Γ is the optical confinement factor per period, N_p is the number of periods, $\hbar \omega$ is the energy of emitted photons, α is the total cavity loss coefficient, and qz is the electric dipole moment of the laser transition.

From the electronic structure calculation results shown in Fig. 4a and b, we have $L_p = 462 \text{ \AA}$ and $z = 66 \text{ \AA}$ for the GaAs structure and $L_p = 199 \text{ \AA}$ and $z = 30 \text{ \AA}$ for the ZnO structure. In both devices, $n_{\text{tot}} = 2 \times 10^{10} \text{ cm}^{-2}$ and $\hbar \omega = 8.2 \text{ eV}$ by design. Incidentally, with this set of parameters the oscillator strength is computed to be 0.63 in the GaAs gain medium and 0.47 in the ZnO structure. For the refractive indices near 2 THz, we use the experimentally determined values of 3.8 and 2.8 for GaAs and ZnO, respectively.^{65,66} Furthermore, from

previously reported measurements with GaAs THz-QC-laser waveguides based on surface plasmons^{5,8} we take $\alpha/\Gamma N_p = 20 \text{ cm}^{-1}$ for both structures considered here.

Regarding the gain line width, γ , a typical value for the GaAs device under study (extrapolated from the literature) is 3 meV.⁶⁵ This can be ascribed partly to lifetime broadening (given the ultrafast, ~ 100 fs, phonon-assisted depopulation of the lower laser states) and partly to broadening due to surface roughness. Using this value in Eq. 3, we calculate for the GaAs structure of Fig. 4a a minimum population inversion required to achieve lasing of $\Delta n_{\text{th}} = 16\%$. The maximum operating temperature correspondingly obtained from the simulation results of Fig. 5 is $T_{\text{max}} \approx 200$ K. This value is reasonably close to the largest working temperature reported to date with GaAs devices, approximately 186 K,⁹ indicating that our model accurately describes the temperature-dependent performance of THz QC lasers.

If we assume $\gamma = 3$ meV also in the ZnO QC gain medium of Fig. 4b we obtain $\Delta n_{\text{th}} = 25\%$ and T_{max} over 300 K. Furthermore, the ability of these devices to operate without cryogenic cooling (i.e., at temperatures accessible with thermoelectric coolers, > 250 K) is predicted for line widths up to over 3.8 meV. Incidentally, in this analysis we have neglected the temperature dependence of the gain line width for simplicity. In any case, this dependence can be expected to be relatively small, again because of the large LO-phonon energies of these materials.

CONCLUSIONS

In summary, we have presented a Monte Carlo study of carrier dynamics versus temperature in two otherwise identical THz QC structures based on GaAs/AlGaAs and ZnO/MgZnO QWs. The simulation results clearly indicate that the ZnO materials system is promising to improve the high-temperature performance of THz injection lasers. In particular, as the temperature is increased from 10 K to 300 K, the population inversion and hence the optical gain are found to decrease by a factor of 4.48 and 1.50 for the AlGaAs and MgZnO structures, respectively. These predictions bear out and quantify the expectation that, the larger the LO-phonon energies (as in going from the AlGaAs to the MgZnO materials system), the more robust the population inversion with respect to thermally activated non-radiative ISB scattering. Furthermore, the simulation results suggest that the ZnO QC structures considered in this work can provide lasing without cryogenic cooling if their gain line width is smaller than about 3.8 meV. While this value appears to be feasible, growth and experimental demonstration of these structures remain considerable challenges. On the other hand, the prospect of operation without cryogenic cooling suggested by this study has

the potential for a revolutionary impact in the general field of THz photonics, and should therefore provide strong impetus for the investigation of these devices.

ACKNOWLEDGEMENTS

This work was supported by the NSF through Grant No. ECCS-0824116 (R. Paiella) and Grant No. ECCS-0901435 (E. Bellotti).

REFERENCES

1. M. Lee and M.C. Wanke, *Science* 316, 64 (2007).
2. R. Köhler, A. Tredicucci, F. Beltram, H.E. Beere, E.H. Linfield, A.G. Davies, D.A. Ritchie, R.C. Iotti, and F. Rossi, *Nature* 417, 156 (2002).
3. R. Paiella, ed., *Intersubband Transitions in Quantum Structures*, 1st ed. (New York: McGraw-Hill, 2006).
4. G. Scalari, L. Ajili, J. Faist, H. Beere, E. Linfield, D. Ritchie, and G. Davies, *Appl. Phys. Lett.* 82, 3165 (2003).
5. B.S. Williams, S. Kumar, Q. Hu, and J.L. Reno, *Opt. Exp.* 13, 3331 (2005).
6. B.S. Williams, S. Kumar, Q. Qin, Q. Hu, and J.L. Reno, *Appl. Phys. Lett.* 88, 261101 (2006).
7. H. Luo, S.R. Laframboise, Z.R. Wasilewski, G.C. Aers, H.C. Liu, and J.C. Cao, *Appl. Phys. Lett.* 90, 041112 (2007).
8. C. Walther, M. Fischer, G. Scalari, R. Terazzi, N. Hoyler, and J. Faist, *Appl. Phys. Lett.* 97, 131122 (2007).
9. S. Kumar, Q. Hu, and L. Reno, *Appl. Phys. Lett.* 94, 131105 (2009).
10. M. Belmoubarik, K. Ohtani, and H. Ohno, *Appl. Phys. Lett.* 92, 191906 (2008).
11. H. Jaffe and D.A. Berlincourt, *Proc. IEEE* 53, 1372 (1965).
12. M. Usuda, N. Hamada, T. Kotani, and M. van Schilfhaarde, *Phys. Rev. B* 66, 125101 (2002).
13. D.C. Reynolds, D.C. Look, B. Jogai, C.W. Litton, G. Cantwell, and W.C. Harsch, *Phys. Rev. B* 60, 2340 (1999).
14. W. Lambrecht, A.V. Rodina, S. Limpijumngong, B. Segall, and B.K. Meyer, *Phys. Rev. B* 65, 075207 (2002).
15. P. Gopal and N. Spaldin, *Polarization, piezoelectric constants and elastic constants of ZnO, MgO and CdO*, <http://www.citebase.org/cgi-bin/citations?id=oai:arXiv.org:cond-mat/0507217> (2005).
16. M. Catti, Y. Noel, and R. Dovesi, *J. Phys. Chem. Solids* 64, 2183 (2003).
17. Y. Noel, C.M. Zicovich-Wilson, B. Civalleri, P. D'Arco, and R. Dovesi, *Phys. Rev. B* 65, 014111 (2001).
18. J.M. Carlsson, *Comput. Mater. Sci.* 22, 24 (2001).
19. J. Serrano, A.H. Romero, F.J. Manjón, R. Lauck, M. Cardona, and A. Rubio, *Phys. Rev. B* 69, 094306 (2004).
20. Z.G. Yu, H. Gong, and P. Wu, *J. Cryst. Growth* 287, 199 (2006).
21. S. Limpijumngong and S. Jungthawan, *Phys. Rev. B* 70, 054104 (2004).
22. A.B. Djurišić, Y. Chan, and E.H. Li, *Appl. Phys. A* 76, 37 (2003).
23. N. Ashkenov, B.N. Mbenkum, C. Bundesmann, V. Riede, M. Lorenz, D. Spemann, E.M. Kaidashev, A. Kasic, M. Schubert, M. Grundmann, G. Wagner, H. Neumann, V. Darakchieva, H. Arwin, and B. Monemar, *J. Appl. Phys.* 93, 126 (2003).
24. C. Klingshirn, H. Priller, M. Decker, J. Bruckner, H. Kalt, R. Hauschild, J. Zeller, A. Waag, A. Bakin, H. Wehmann, K. Thonke, R. Sauer, R. Kling, F. Reuss, and Ch. Kirchner, *Adv. Solid State Phys.* 45, 275 (2005).
25. D.C. Look, *Semicond. Sci. Technol.* 20, S55 (2005).
26. C.-Y. Ren, S.-H. Chiou, and C.-S. Hsue, *Physica B* 349, 136 (2004).
27. J.G. Lu, Y.Z. Zhang, Z.Z. Ye, L.P. Zhu, L. Wang, B.H. Zhao, and Q.L. Liang, *Appl. Phys. Lett.* 88, 222114 (2006).
28. L.J. Mandalapu, F.X. Xiu, Z. Yang, and J.L. Liu, *J. Appl. Phys.* 102, 023716 (2007).

29. Y.R. Ryu, S. Zhu, D.C. Look, J.M. Wrobel, H.M. Jeong, and H.W. White, *J. Cryst. Growth* 216, 330 (2000).
30. Y.R. Ryu, T.S. Lee, J.H. Leem, and H.W. White, *Appl. Phys. Lett.* 83, 4032 (2003).
31. Y.J. Zeng, Z.Z. Ye, W.Z. Xu, L.L. Chen, D.Y. Li, L.P. Zhu, B.H. Zhao, and Y.L. Hu, *J. Cryst. Growth* 283, 180 (2005).
32. D.C. Look, D.C. Reynolds, J.R. Sizelove, R.L. Jones, C.W. Litton, G. Cantwell, and W.C. Harsch, *Solid State Commun.* 105, 339 (1998).
33. J.D. Albrecht, P.P. Ruden, S. Limpijumngong, W.R.L. Lambrecht, and K.F. Brennan, *J. Appl. Phys.* 86, 6864 (1999).
34. T. Makino, Y. Segawa, A. Tsukazaki, A. Ohtomo, and M. Kawasaki, *Appl. Phys. Lett.* 87, 022101 (2005).
35. F. Bertazzi, M. Goano, and E. Bellotti, *J. Electron. Mater.* 36, 857 (2007).
36. E. Furno, F. Bertazzi, M. Goano, G. Ghione, and E. Bellotti, *Solid-State Electron.* 52, 1796 (2008).
37. T. Makino, Y. Segawa, M. Kawasaki, A. Ohtomo, R. Shiroki, K. Tamura, T. Yasuda, and H. Koinuma, *Appl. Phys. Lett.* 78, 1237 (2001).
38. Y.R. Ryu, T.S. Lee, J.A. Lubguban, A.B. Corman, H.W. White, J.H. Leem, M.S. Han, Y.S. Park, C.J. Youn, and W.J. Kim, *Appl. Phys. Lett.* 88, 052103 (2006).
39. C. Persoon, C. Platzer-Björkman, J. Malmström, T. Törndhal, and M. Edoff, *Phys. Rev. Lett.* 97, 146403 (2006).
40. B. Sanders and A. Kitai, *Chem. Mater.* 4, 1005 (1992).
41. Y. Yoo, Z. Jin, T. Chikyow, T. Fukumura, K. Kawasaki, and H. Koinuma, *Appl. Phys. Lett.* 81, 3798 (2002).
42. B. Meyer, A. Polity, B. Farangis, Y. He, D. Hasselkamp, and T.C. Wang, *Appl. Phys. Lett.* 85, 4929 (2001).
43. B. Meyer, A. Polity, B. Farangis, Y. He, D. Hasselkamp, T.C. Wang, U. Haboek, and A. Hoffman, *Phys. Stat. Sol. (c)* 1, 694 (2004).
44. A. Polity, B. Meyer, T.C. Wang, U. Haboek, and A. Hoffman, *Phys. Stat. Sol. (c)* 203, 2867 (2006).
45. A. Ohtomo, M. Kawasaki, T. Koida, K. Masubuchi, H. Koinuma, Y. Sakurai, Y. Yoshida, T. Yasuda, and Y. Segawa, *Appl. Phys. Lett.* 72, 2466 (1998).
46. W. Park, G.-C. Yi, and H. Jang, *Appl. Phys. Lett.* 79, 2022 (2001).
47. A. Sharma, J. Narajan, J. Muth, C. Teng, C. Jin, A. Kwit, R. Kolbas, and O. Holland, *Appl. Phys. Lett.* 75, 3327 (1999).
48. C.W. Teng, J.F. Muth, Ü. Özgür, M.J. Bergmann, H.O. Everitt, A.K. Sharma, C. Jin, and J. Narayan, *Appl. Phys. Lett.* 76, 979 (2000).
49. I. Takeuchi, W. Yang, K. Chang, M.A. Aronova, T. Venkatesan, R. Vispute, and L. Bendersky, *J. Appl. Phys.* 94, 7336 (2003).
50. T. Gruber, C. Kirchner, R. Kling, F. Reuss, and A. Waag, *Appl. Phys. Lett.* 84, 5359 (2004).
51. D. Ma, Z. Ye, and L. Chen, *Phys. Stat. Sol. (a)* 201, 2929 (2004).
52. T. Gruber, C. Kirchner, R. Kling, F. Reuss, A. Waag, F. Bertram, D. Foster, J. Christen, and M. Schreck, *Appl. Phys. Lett.* 83, 3290 (2003).
53. O. Vigil, L. Vaillant, F. Cruz, G. Santana, A. Morales-Acevedo, and G. Contreras-Puente, *Thin Solid Films* 361, 53 (2000).
54. M.S. Han, J.H. Kim, T.S. Jeong, J.M. Park, C.J. Youn, J.H. Leem, and Y.R. Ryu, *J. Cryst. Growth* 303, 506 (2007).
55. F. Koffyberg, *Phys. Rev. B* 13, 4470 (1976).
56. A. Ashrafi, H. Kumano, I. Suemune, Y. Ok, and T. Seong, *J. Cryst. Growth* 237, 518 (2002).
57. E. Bellotti, K. Driscoll, T.D. Moustakas, and R. Paiella, *J. Appl. Phys.* 105, 113103 (2009).
58. J. Lu and J. Cao, *Appl. Phys. Lett.* 88, 061119 (2006).
59. C. Jirauschek, G. Scarpa, P. Lugli, M. Vitiello, and G. Scamarcio, *Appl. Phys. Lett.* 101, 086109 (2007).
60. O. Bonno, J.-L. Thobel, and F. Dessenne, *J. Appl. Phys.* 97, 043702 (2005).
61. S.M. Goodnick and P. Lugli, *Phys. Rev. B* 37, 2578 (1988).
62. M. Mosko and A. Moskova, *Phys. Rev. B* 44, 10794 (1991).
63. M. Mosko, A. Moskova, and V. Cambel, *Phys. Rev. B* 51, 16860 (1995).
64. C. Sirtori and R. Teissier, *Intersubband Transitions in Quantum Structures*, ed. R. Paiella (New York: McGraw-Hill, 2006), pp. 1–39.
65. H. Callebout, S. Kumar, B.S. Williams, Q. Qin, Q. Hu, and J.L. Reno, *Appl. Phys. Lett.* 83, 207 (2003).
66. J. Han, Z. Zhu, S. Ray, A. K. Azad, W. Zhang, and M. He, *Appl. Phys. Lett.* 89, 031107 (2006).